




ANALYSIS OF HEMODYNAMIC IMPACTS  
ON TWO-LAYER BLOOD FLOW  
IN A TRAPEZOIDAL STENOSIS WITHIN AN ARTERY

Subedi S.Sh., Gautam P.N.<sup>1</sup>, Kafle J.

**Abstract** The enigma of blood circulation through a trapezoidal narrowing in arteries has been explored. Blood flow has been depicted using a sophisticated two-layered model comprising a central zone filled with suspended blood cells and a surrounding peripheral layer of plasma. Using an analytical approach, the study of a steady flow in a restricted artery with two-layered blood flow has been comprehensively investigated. Mathematical formulae describing hemodynamic characteristics of a binal-layer system, including the velocity distribution and volumetric flow rate, as well as the influence of stenosis growth on these elements, have been created, taking into account changes in the core and peripheral layers' viscosity coefficients. Pressure and shear stress ratio in arteries with and without stenosis are also calculated analytically. Blood has higher velocity in the two-layer model compared to the single-layer model. The rate of volumetric flow reduces as the viscosity rises. The topmost value of pressure drop and shear stress is achieved at the peak of stenosis height. This modeling approach has an appeal to researchers in cardiology, biomechanics, and related fields.

**Keywords:** Dual-layer, Peripheral, Core, Mesa, Viscosity, Axial length.

**AMS Mathematics Subject Classification:** 76.

**DOI:** 10.32523/2306-6172-2025-13-3-97-111.

## 1 Introduction

Blood is a unique biological fluid. Blood contains four elementary components: plasma, red blood cells, white blood cells, and platelets. Blood has a range of functions, including transporting oxygen and vital nutrients to the body's tissues and organs, and forming clots to avoid hemorrhaging [1]. According to the WHO, 38% of the 17 million premature deaths from noncommunicable diseases in 2019 were caused by cardiovascular diseases (CVDs). CVDs are expected to remain the leading cause of global mortality, with 23.3 million deaths projected by 2030 [2]. The majority of these demises stem from coronary heart disease, a condition affecting the blood vessels that nurture the heart muscle, or cerebrovascular disease, which impacts the blood vessels supplying the brain. Consequently, the obstruction of blood flow to the heart or brain commonly triggers the onset of a heart attack or stroke, respectively [3]. A key determinant contributing to the prevalence of these two categories of cardiovascular diseases is the existence of stenosis within the blood vessels. Under unhealthy conditions, an unusual growth that occurs in any part of the cardiovascular system, causing a narrowing in a body, tube, opening, or pathway, is known in the medical field as stenosis [4]. Another term for it is coarctation, but this is typically only used about aortic coarctation. Stenosis can boost the flow of blood impedance in an artery, causing blood pressure to rise. Furthermore, constriction can grow over time and frequently leads to a disease called arterial thrombosis, which is the formation of a blood plaque in blood arteries, restricting the supply of blood to distinct areas of the human body [5]. The actual cause of stenosis is unknown, however,

---

<sup>1</sup>Corresponding Author.

numerous researchers have empirically as well as theoretically scrutinized the impact that narrowing on blood flow traits such as velocity, resistance on the skin, and resilient impedance by treating blood as a liquid that follows Newton's laws. Blood, on the other hand, is classified as a non-Newtonian fluid that moves at low shear rates via tiny blood vessels [6].

After the pioneering study conducted by Mann, Hennrick, Essex, and Blades in [7], a multitude of researchers have thoroughly explored the effects of stenosis on the characteristics of blood flow. Notable studies include those by Young [4], MacDonald [9], Haldar [8], Bitoun and Bellet [11], Chakravarty [10]. Pushpa et.al. [5], conducted a detailed examination to study the impact of increasing stenosis on the flow of blood within the vessels which delved into the dynamic changes in hemodynamics that occur as stenosis progresses gradually. Absaar et al. [12], analyzed pulsatile blood flow around several plaque shapes, including trapezoidal, ellipsoidal, and triangular. Keshavarz, et al. and Lee [13, 14] investigated pulsed blood transit in curved arteries with varying levels of stenosis. The effect of spiral blood flow on restricted arteries. Jeevan Kafle et al. [15], investigated the mathematical analysis of the hemodynamic parameters of blood flow in an artery.

The aforementioned literature examines the structure of arteries, considering them to be composed of a single layer. Numerous scholars have examined the dynamics of blood flow within arteries by classifying blood as either Newtonian or non-Newtonian fluids. Because blood is a mixture of red cells within the plasma, it demonstrates non-Newtonian behavior at low shear rates, with a non-zero yield stress at this point. Bugliarello and Sevilla [16], Cokelet [17], and Thurston [18], carried out researches that demonstrated the presence of a plasma layer devoid of cells near the vessel walls, alongside a core region where all erythrocytes are suspended in plasma. Hence, a precise representation of the circulation of blood in tiny vessels should integrate dual-layered model. J. B. Shukla [19], adopting this theory suggests that the peripheral membrane has a role in the operation of the vascular system. Ponalagusamy [20], studied the viscosity of blood flow with a dual-layer model and examined the impact of minor stenosis on blood flow variables using theoretical and numerical methods. Chaturani and Kaloni [21], proposed a dual-layered model with stresses at the core layer, assuming blood as an incompressible fluid. Biswas and Chakraborty [23], have studied blood as a two-layered and Bingham plastic in nature, and separate equations are derived for these two fluids using the perturbation method. Singh et al. [22], have successfully created a blood flow model specifically designed for arteries that contain multiple, and non-uniform stenosis formations along their radial direction.

A commendable effort is made in this theoretical study to investigate a few of the significant features of the two-layered Newtonian rheology of blood flowing through a tapering artery when trapezoidal stenosis is present. Given that the morphology of stenosis varies in manifestation, studying trapezoidal shape stenosis is significant. As the peripheral layer and the red blood cells in the plasma can no longer be ignored, the two-layered blood flow model offers a more accurate representation of flow in arteries. With trapezoidal stenosis present, this model enables the evaluation of the impact of the hematocrit, stenosis height, and peripheral layer on the blood flow characteristics. One may observe the detrimental impact that this constriction has on the cardiovascular system's arteries.

## 2 Two layered blood flow model for the trapezoidal shape of stenosis

This article examines a dual-layer framework for steady, laminar, and axis-symmetric flow in a coronary with trapezoidal stenosis, potentially improving knowledge of blood flow. We considered that blood is compressible and Newtonian fluid in the stenosed artery. The rationale

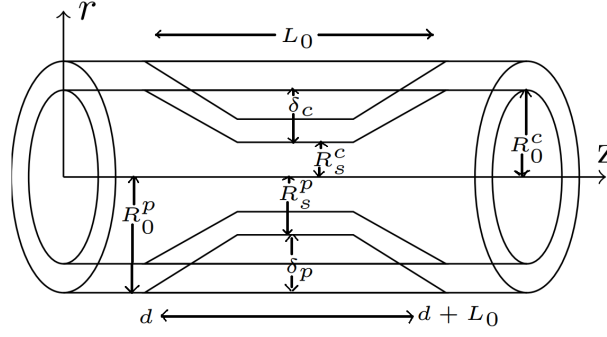


Figure 1: Part of the artery with stenosis.

for considering blood as a Newtonian fluid in this case is due to the substantial size of the arteries, which measure 1.2 mm. The Navier-Stokes equation [24], is often used to represent the circulation in arteries. Assume a uniform, cylindrical, axisymmetric, laminar blood flow that is stable and fully formed via the artery of radius  $R_0$  in the presence of trapezoidal stenosis. Let  $r$  denote the radial velocity function and  $p$  symbolize the pressure. The velocities within a cylindrical artery are characterized by three facets:  $w^r$ ,  $w^\theta$ , and  $w^z$ . Consequently, the continuity equation can be expressed in the following manner [24].

$$\frac{1}{r} \frac{\partial}{\partial r}(r w^r) + \frac{\partial}{\partial z}(w^z) = 0 \quad (1)$$

The equation of Navier-Stokes as it pertains to the radial and z-axis is,

$$\rho \left( \frac{\partial w^r}{\partial t} + w^r \frac{\partial w^r}{\partial r} + w^z \frac{\partial w^r}{\partial z} \right) = -\frac{\partial p}{\partial r} + \mu \left( \frac{\partial^2 w^r}{\partial r^2} + \frac{\partial^2 w^r}{\partial z^2} + \frac{1}{r} \frac{\partial w^r}{\partial r} - \frac{w^r}{r^2} \right) \quad (2)$$

$$\rho \left( \frac{\partial w^z}{\partial t} + w^r \frac{\partial w^z}{\partial r} + w^z \frac{\partial w^z}{\partial z} \right) = -\frac{\partial p}{\partial z} + \mu \left( \frac{\partial^2 w^z}{\partial r^2} + \frac{\partial^2 w^z}{\partial z^2} + \frac{1}{r} \frac{\partial w^z}{\partial r} \right) \quad (3)$$

In the case of axisymmetric flow, both  $w^r$  and  $w^\theta$  are zero, and  $\frac{\partial w^z}{\partial z}$  is also zero due to the steady flow along the z-axis. When  $w^z$  is simplified as  $w$ , equation (3) is then reduced.

$$0 = -\frac{\partial p}{\partial z} + \frac{1}{r} \left\{ \mu(r) r \frac{\partial w}{\partial r} \right\} \quad (4)$$

Where  $\mu(r)$  represents the blood's viscosity coefficient. Blood is depicted here as dual layers, a core layer at the center and an outward peripheral layer, each with its own set of homodynamic characteristics. In the realm of peripheral and core layers, the labels p and c are designated, while the suffixes 0 and s distinguish between stenotic and non-stenotic areas.

## 2.1 Configuration of the stenosis

Given that the viscosities of the core and peripheral layer are  $\mu_p$  and  $\mu_c$ , accordingly. The viscosity coefficient  $\mu(r)$  can be expressed as follows:

$$\mu(r) = \begin{cases} \mu_p, & \text{if } R_s^c(z) \leq r \leq R_s^p(z), \\ \mu_c, & \text{if } 0 \leq r \leq R_s^c(z). \end{cases} \quad (5)$$

The core radii ( $R_s^c$ ,  $R_0^c$ ) and peripheral radii ( $R_s^p$ ,  $R_0^p$ ) of the artery with stenosis and without stenosis portions correspondingly. Assume that the maximum height of stenosis in the peripheral and core layers, respectively, is represented by  $\delta_p$  and  $\delta_c$ .

According to Ponalagusamy [20], the stenosis's geometry for the periphery layers as,

$$\frac{R_s^p}{R_0^p} = \begin{cases} 1 - \frac{4\delta_p}{(R_0^p)^2}z, & \text{if } 0 \leq z \leq \frac{L_0}{4}, \\ 1 - \frac{\delta_p L_0}{(R_0^p)^2}, & \text{if } \frac{L_0}{4} \leq z \leq \frac{3L_0}{4}, \\ 1 - \frac{4\delta_p}{(R_0^p)^2}(L_0 - z), & \text{if } \frac{3L_0}{4} \leq z \leq L_0, \\ 1, & \text{otherwise.} \end{cases} \quad (6)$$

Similarly, According to Ponalagusamy [20], the stenosis's geometry for the core layers as,

$$\frac{R_s^c}{R_0^c} = \begin{cases} 1 - \frac{4\delta_c}{(R_0^c)^2}(z), & \text{if } 0 \leq z \leq \frac{L_0}{4}, \\ 1 - \frac{\delta_c L_0}{(R_0^c)^2}, & \text{if } \frac{L_0}{4} \leq z \leq \frac{3L_0}{4}, \\ 1 - \frac{4\delta_c}{(R_0^c)^2}(L_0 - z), & \text{if } \frac{3L_0}{4} \leq z \leq L_0, \\ 1, & \text{otherwise.} \end{cases} \quad (7)$$

The suitable boundary condition for this issue may be expressed as [25],

$$\frac{\partial w_c}{\partial r} = 0 \quad \text{at } r = 0; \quad w_p = w_c \quad \text{at } r = R_s^c \quad (8)$$

### 3 The velocity distribution of blood flow in an artery

Peripheral layered velocity: Let  $w_p$  be the velocity peripheral layer [i.e. region  $R_s^c \leq r \leq R_s^p$ ]. Then, equation 4 on integrating and applying boundary condition of 8 becomes

$$w_p = \frac{P}{4\mu_p} ((R_s^p)^2 - r^2) \quad \text{for } R_s^c \leq r \leq R_s^p. \quad (9)$$

Core layered velocity: Next, suppose  $w_c$  be velocity of core layer [i.e. region  $0 \leq r \leq R_s^c(z)$ ]. Then, from Eq. 4,

$$-P(z) \frac{r}{\mu_c} = \frac{\partial}{\partial r} \left( r \frac{\partial w_c}{\partial r} \right) \quad (10)$$

On integrating and applying the boundary condition of 8. We get,

$$-P(z) \frac{r^2}{2\mu_c} = r \frac{\partial w_c}{\partial r} + D(z) \quad (11)$$

Now we integrate and apply boundary conditions for the core layer in the region  $0 \leq r \leq R_s^c(z)$  we get,

$$w_c = \frac{P}{4\mu_p} \left[ ((R_s^p)^2 - (R_s^c)^2) + \frac{\mu_p}{\mu_c} ((R_s^c)^2 - r^2) \right]. \quad (12)$$

### 4 Volumetric flow rate

Peripheral volumetric flow rate

$$Q_p = \int_{R_s^c}^{R_s^p} 2\pi r w_p dr = 2\pi \frac{P}{4\mu_p} \int_{R_s^c}^{R_s^p} (r(R_s^p)^2 - rr^2) dr = \frac{\pi P}{8\mu_p} ((R_s^p)^2 - (R_s^c)^2)^2. \quad (13)$$

Core layered volumetric flow rate:

$$Q_c = \int_0^{R_s^c} 2\pi r w_c dr = \frac{\pi P}{8\mu_p} \left[ 2(R_s^c)^2 \left[ (R_s^p)^2 - \left(1 - \frac{\mu_k}{2}\right) (R_s^c)^2 \right] \right], \quad (14)$$

where  $\mu_k = \mu_c/\mu_p$ .

Total volumetric flow rate: The entire volumetric flow rate ( $Q$ ) is a combination of the volumetric rates of the peripheral layer ( $Q_p$ ) and the core layer ( $Q_c$ ). Then, the total volumetric rate is

$$Q = Q_p + Q_c = \frac{\pi P}{8\mu_p} \left[ (R_s^p)^4 - (1 - \mu_k) (R_s^c)^4 \right]. \quad (15)$$

#### 4.1 Shear stress and its ratio

Peripheral stress:

$$\tau_s^p = \left[ -\mu_p \frac{\partial v_p}{\partial r} \right]_{r=R_s^p} = \left[ -\mu_p (-P(z)) \frac{r}{2\mu_p} \right]_{r=R_s^p} = \left[ P(z) \frac{R_s^p}{2} \right] \quad (16)$$

putting the value of  $P(z)$  from 13 we get

$$\tau_s^p = \frac{4Q_p\mu_p \left( \frac{R_s^p}{R_0^p} \right)}{\pi(R_0^p)^3(1 - \beta^2)^2} \left[ \frac{R_s^p}{R_0^p} \right]^{-4}. \quad (17)$$

when there is no stenosis  $\delta_P = 0$

$$\tau_0^p = \frac{4Q_p\mu_p}{\pi(R_0^p)^3(1 - \beta^2)^2}. \quad (18)$$

So the ratio is

$$\frac{\tau_s^p}{\tau_0^p} = \left[ \frac{R_s^p}{R_0^p} \right]^{-3}. \quad (19)$$

Core stress:

$$\tau_s^c = \left[ -\mu_c \frac{\partial v_c}{\partial r} \right]_{r=R_s^c} = \left[ -\mu_c (-P(z)) \frac{r}{2\mu_c} \right]_{r=R_s^c} = \left[ P(z) \frac{R_s^c}{2} \right]. \quad (20)$$

Putting the value of  $P(z)$  from (9)

$$\tau_s^c = \frac{2\mu_p Q_c}{\pi(R_0^c)^3} \left( \frac{R_s^c}{R_0^c} \right)^{-3} \left[ \frac{1}{\beta^2} - \left(1 - \frac{\mu_k}{2}\right) \right]^{-1}, \quad (21)$$

similarly

$$\tau_0^c = \frac{2\mu_p Q_c}{\pi(R_0^c)^3} \left[ \frac{1}{\beta^2} - \left(1 - \frac{\mu_k}{2}\right) \right]^{-1} \quad (22)$$

core stress ratio is

$$\frac{\tau_s^c}{\tau_0^c} = \left[ \frac{R_s^c}{R_0^c} \right]^{-3}. \quad (23)$$

## 4.2 Pressure and its ratio

Peripheral pressure and its ratio

$$(\Delta p)_s^p = \int_0^{L_0} \left( \frac{-dp}{dz} \right) dz = \frac{8\mu_p Q_p}{\pi (R_0^p)^4} \int_0^{L_0} \left[ \left( \frac{R_s^p}{R_0^p} \right)^2 - \left( \frac{R_s^c}{R_0^p} \right)^2 \right]^{-2} dz \quad (24)$$

We have

$$\Delta p_s^p = (\Delta p_s^p)_1 + (\Delta p_s^p)_2 + (\Delta p_s^p)_3 \quad (25)$$

where

$$(\Delta p_s^p)_1 = \int_0^{L_0/4} \frac{8\mu_p Q_p}{\pi (R_0^p)^4 (1 - \beta^2)^2} \left( 1 - \frac{4\delta_p z}{(R_0^p)^2} \right)^{-4} dz \quad (26)$$

$$(\Delta p_s^p)_2 = \int_{L_0/4}^{3L_0/4} \frac{8\mu_p Q_p}{\pi (R_0^p)^4 (1 - \beta^2)^2} \left( 1 - \frac{\delta_p L_0}{(R_0^p)^2} \right)^{-4} dz \quad (27)$$

$$(\Delta p_s^p)_3 = \int_{3L_0/4}^{L_0} \frac{8\mu_p Q_p}{\pi (R_0^p)^4 (1 - \beta^2)^2} \left( 1 - \frac{4\delta_p (L_0 - z)}{(R_0^p)^2} \right)^{-4} dz \quad (28)$$

Integrating (26), (27), and (28) and putting the value in (25) we have,

$$(\Delta p_s^p) = \frac{4\mu_p Q_p L_0}{\pi (R_0^p)^4 (1 - \beta^2)^2} \left[ \left( 1 - \frac{\delta_p L_0}{(R_0^p)^2} \right)^{-4} + 1 + 2 \left( \frac{\delta_p L_0}{(R_0^p)^2} \right) + \frac{10}{3} \left( \frac{\delta_p L_0}{(R_0^p)^2} \right)^2 \right] \quad (29)$$

Similarly,

$$(\Delta p_0^p) = \frac{8\mu_p Q_p}{\pi (R_0^p)^4 (1 - \beta^2)^2} L_0 \quad (30)$$

so we calculate its ratio as

$$\frac{\Delta p_s^p}{\Delta p_0^p} = \frac{1}{2} \left[ \left( 1 - \frac{\delta_p L_0}{(R_0^p)^2} \right)^{-4} + 1 + 2 \left( \frac{\delta_p L_0}{(R_0^p)^2} \right) + \frac{10}{3} \left( \frac{\delta_p L_0}{(R_0^p)^2} \right)^2 \right], \quad (31)$$

### Core Pressure ratio

$$\frac{\Delta p_s^c}{\Delta p_0^c} = \frac{1}{2} \left[ \left( 1 - \frac{\delta_c L_0}{(R_0^c)^2} \right)^{-4} + 1 + 2 \left( \frac{\delta_c L_0}{(R_0^c)^2} \right) + \frac{10}{3} \left( \frac{\delta_c L_0}{(R_0^c)^2} \right)^2 \right]. \quad (32)$$

## 5 Result and Discussion

The trapezoidal model currently in use has been specifically designed and refined to examine various characteristics and aspects of blood circulation within an artery that is affected by stenosis, providing valuable insights into the dynamics of this common vascular condition. Cogent solutions of the celerity profile, volumetric flow rate, ratio of pressure, shear stress ratio, and effective viscosity on the above-mentioned aspects are scrutinized. Computational software has been used to obtain the result. The parameters that are taken into consideration are the pressure gradient  $P = 120$  mmHg, the peripheral viscosity  $\mu_p = 1.4$  cP, the core viscosity  $\mu_c = 4$  cP, the peripheral radius  $R_0^p = 1.2$  mm, the core radius  $R_0^c = 0.9$  mm, the periphery stenotic height  $\delta_p = 0.3$  mm, and the core stenotic height  $\delta_c = 0.05$  mm if not mentioned.

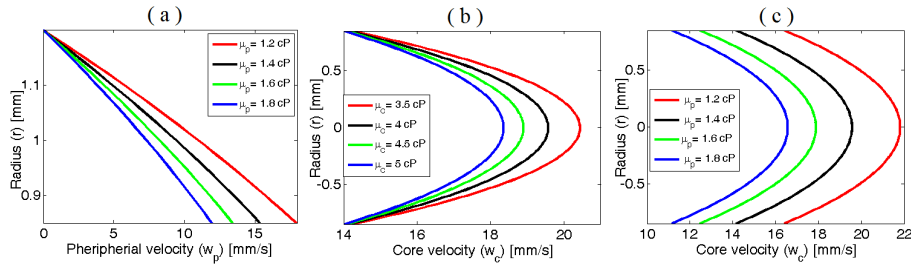


Figure 2: a: Peripheral Velocity ( $w_p$ ) for varying periphery viscosity  $\mu_p$ , b: Core velocity ( $w_c$ ) for varying core viscosity  $\mu_c$ , c: Core velocity ( $w_c$ ) for varying periphery viscosity  $\mu_p$ .

## 5.1 The velocity account of blood flow through a narrowed artery.

### 5.1.1 Analysis of peripheral velocity

Figure 2a shows a plot of velocity in the peripheral layer vs radius ( $r$ ). The radius ( $r$ ) of peripheral velocity ranges from 0.85 mm to 1.2 mm. As in Fig. 2a velocity is zero at  $r = 1.2$  mm, which is the artery's inner wall. Eventually, the decrease in size of  $r$  causes an increase in velocity, as seen in the Tab. 1. Finally, at  $r=0.85$  mm, velocity reaches 17.94 mm/s, 15.38 mm/s, 13.45 mm/s, and 11.96 mm/s for viscosity of 1.2 cP, 1.4 cP, 1.6 cP, and 1.8 cP, respectively. With a rise in viscosity of 0.6 cP, the speed dwindles by 1.92 mm/s, 3.67 mm/s, 5.25 mm/s, and 5.98 mm/s for  $r$  values of 1.1 mm, 1 mm, 0.9 mm, and 0.85 mm respectively. The speed reduction is notably higher for smaller  $r$  when juxtaposed with larger  $r$ . In a nutshell velocity and viscosity dance in a mesmerizing inverse relationship, just like the graceful waltz of radius ( $r$ ). The acceleration of velocity experiences a swift surge as  $r$  shrinks elegantly.

Table 1: Table with radius and viscosity values along with corresponding velocities

Radius (r) [mm]	Velocity ( $w_p$ ) [mm/s]				Total change in velocity
	Viscosity ( $\mu_p$ ) [cP]				
	1.20	1.40	1.60	1.80	
1.10	5.75	4.46	4.31	3.83	1.92
1.00	11.00	9.43	8.25	7.33	3.67
0.90	15.75	13.50	11.81	10.50	5.25
0.85	17.94	15.38	13.45	11.96	5.98

### 5.1.2 Analysis of Core velocity

Figure 2 b and 2 c illustrate the relationship concerning the core layer velocity for varying core and peripheral layer viscosity, respectively. The radius ( $r$ ) ranges from -0.85 mm to 0.85 mm. In Fig. 2 c by considering an average core viscosity of  $\mu_c = 4$  cP with peripheral viscosities of 1.2 cP, 1.4 cP, 1.6 cP, and 1.8 cP, the maximum velocities are observed to be 21.82 mm/s, 19.57 mm/s, 17.89 mm/s, and 16.57 mm/s, respectively at  $r=0$ . Initiating from  $r=0.85$  mm where the velocity is 16.41 mm/s, 14.16 mm/s, 12.47 mm/s, 11.16 mm/s, a consistent increase of 3.54 mm/s is noted with a decrease in  $r$  by 0.35 mm for all scenarios. On the contrary, a reduction in  $r$  by 0.5 mm (from 0.5 mm to 0 mm) results in a velocity increment of 1.87 mm/s. In summary, it can be deduced that viscosity and velocity exhibit an inverse relationship as expected, and the velocity increment towards the center is slightly gradual. Remarkably, the increment remains constant irrespective of viscosity, resulting in a total velocity increase of 5.41 mm/s while transitioning from  $r=0.85$  mm toward the artery center.

Similarly, Fig. 2 b depicts an estimation of an average peripheral viscosity at  $\mu_p = 1.4$

cP while the core viscosities are 3.5 cP, 4 cP, 4.5 cP, and 5 cP. Correspondingly, at  $r=0.85$  mm, the velocities display values of 14.25 mm/s, 14.16 mm/s, 14.08 mm/s, and 14.03 mm/s respectively based on the aforementioned viscosities. Notably, a noticeable increase of 2.83 mm/s, 3.15 mm/s, 3.54 mm/s, and 4.05 mm/s is observed in velocity as the transition is made from  $r = 0.85$  mm to  $r = 0.5$  mm. At the core of the artery, the velocity peaks, reaching values of 20.44 mm/s, 19.57 mm/s, 18.90 mm/s, and 18.36 mm/s for the respective core viscosity ( $\mu_c = 3.5, 4, 4.5, 5$ ) cP. In light of the above findings, it can be inferred that alterations in peripheral viscosity have a more pronounced impact on velocity compared to variations in core viscosity.

### 5.1.3 Analysis of 3-D velocity figure

Figure 3 visualizes velocity ( $w$ ) with different viscosity ( $\mu$ ) and radial distance ( $r$ ). The color bar represents the intensity of velocity, with red being greater and blue representing lower. In all three pictures, velocity is lower near the wall and greater towards the center, and lower viscosity produces more reddish hue than higher viscosity. Fig. 3 a and Fig. 3 b are curved when compared to Fig. 3 c, and the velocity of blood is higher in the core layer, exceeding 20 mm/s starting at 14 mm/s, but the peripheral layer velocity starts at 0 (at the walls) and can reach approximately 16 mm/s. So, we may deduce that the core layer has a higher velocity than the periphery layer resulting in the artery a favorable situation for the deposition of erythrocytes. This is visible because the core layer is located toward the center of the artery, where blood velocity is high.

### 5.1.4 Two-layer velocity overview of blood flow in a stenotic artery. The contrast of velocity profiles for single and dual layers

Here viscosity is deemed 3.5 cP in single-layer and in two-layer peripheral viscosity is considered 1.4 cP and core viscosity is reckoned 3.5 cP. Fig. 4a, compares velocity patterns in dual-layer and a single-layer blood flow for radial distances ranging from 0.0 to 1.2 mm. At a radial distance of 0.85 mm, the two-layered velocity is 15.38 mm/s compared to 6.15 mm/s for single layers. At a radial distance of 0.5 mm, the velocity is 19.43 mm/s and 10.2 mm/s in both layers, respectively. The center speed is 21.57 mm/s for two layers and 12.34 mm/s for a single layer. Single-layered velocity is seen to be parabolic, but in double layer peripheral velocity is somewhat lined up, but the core velocity is also parabolic. Fig. 4b, portrays single-layered blood flow with varied radial spacing (0.0-1.2 mm). The speed is 12.34 mm/s at the center, 10.20 mm/s at the value of 0.5 mm, 6.15 mm/s at the value of 0.85 mm, and 3.77 mm/s at the value of 1 mm. It is found that the artery's core experiences the greatest velocity of 12.34 mm/s, while its wall experiences the minimum velocity of 3.77 mm/s. For a radial distance of values (0.0-1.2) mm, the velocity distribution in a double-layered blood flow is shown in Fig. 4c. The velocity is 21.57 mm/s at the center, 19.43 mm/s at 0.5 mm, 15.38 mm/s at 0.85 mm, and 5.429 mm/s at 1 mm. It can be observed that the central core layer has the highest velocity, measuring 21.57 mm/s. In the peripheral layer, velocity in the vicinity of the artery wall reaches its minimum value of 15.328 mm/s. The conclusion is that velocity rises as stenosis thickness in both layers grows, although two-layered blood flow showed greater velocities than single-layered blood flow.

## 5.2 The volumetric flow rate of blood flow via a stenotic artery

### 5.2.1 Analysis of the peripheral layer volume flow rate

For varying viscosity ( $\mu_p$ ) and for different pressure periphery volume flow rate is plotted in Fig. 5c. The maximum volumetric flow rate of  $16.24 \text{ mm}^3/\text{s}$  is observed at lower viscosity



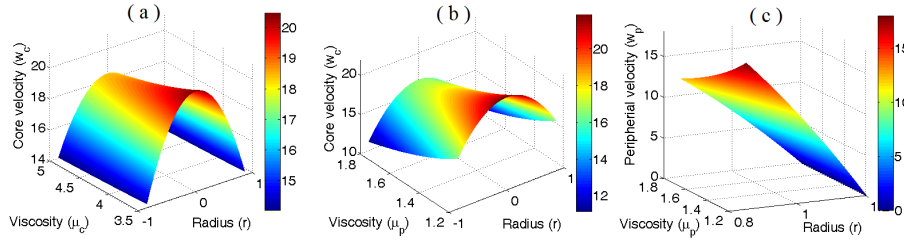


Figure 3: a: Core Velocity ( $w_c$ ) for varying core viscosity  $\mu_c$ , b: Core velocity ( $w_c$ ) for varying periphery viscosity  $\mu_p$ , c: Peripheral Velocity ( $w_p$ ) for varying periphery viscosity  $\mu_p$ .

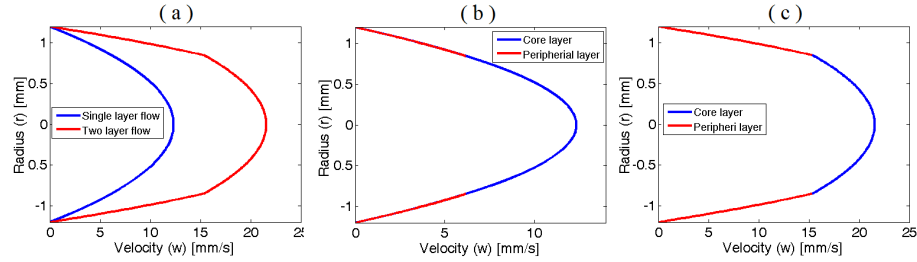


Figure 4: Velocity distribution a: Single-layered versus dual-layered model, b: Single layered model, c: Dual-layered Model.

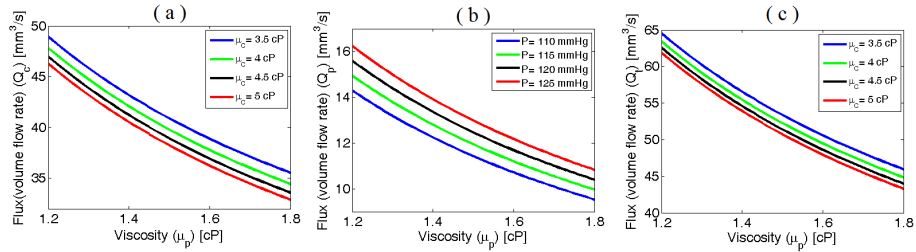


Figure 5: a: Volumetric flow rate in core layer ( $Q_c$ ), b: Total volumetric flow rate ( $Q_t$ ), c: Volumetric flow rate in periphery layer ( $Q_p$ ).

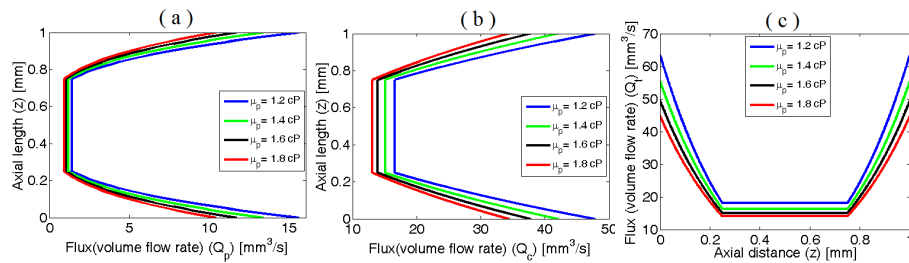


Figure 6: Volumetric flow rate along axial direction a: Periphery volumetric flow rate ( $Q_p$ ), b: Core volumetric flow rate ( $Q_c$ ), c: Total volumetric flow rate ( $Q_t$ ).

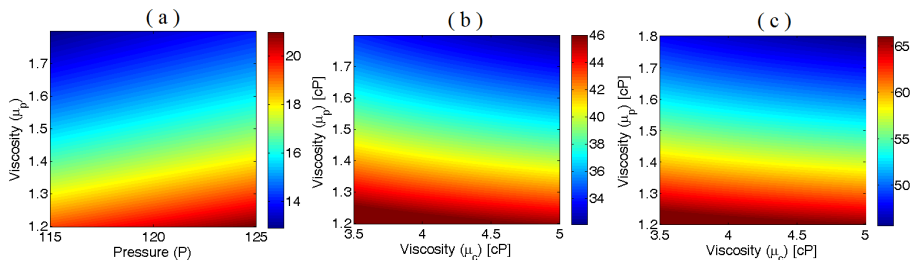


Figure 7: 3-D visualization a: Volumetric flow rate in peripheral layer, b: Volumetric flow rate in core layer, c: Total volumetric flow rate.

and higher pressure ( $\mu_p = 1.2$  cP and  $p=125$  mmHg), whereas the minimum volumetric flow rate is observed at  $9.53 \text{ mm}^3/\text{s}$  flow lower pressure and higher viscosity ( $\mu_p = 1.8$  cP and  $p=115$  mmHg). As viscosity increases by  $0.6$  cP, volumetric flow decreases by roughly  $33.35\%$  across all pressures in Fig. 5c. Increasing pressure by  $15$  mmHg leads to an approximately  $13.6\%$  increase in flow rate across all viscosities in Fig. 5c. This indicates that the peripheral volumetric flow rate is inversely proportional to viscosity and directly related to pressure.

As in Fig. 6a, when devoid of any constriction, the volumetric flow rate on the periphery showcases a mesmerizing sequence:  $15.59 \text{ mm}^3/\text{s}$ ,  $13.36 \text{ mm}^3/\text{s}$ ,  $11.69 \text{ mm}^3/\text{s}$ ,  $10.39 \text{ mm}^3/\text{s}$ , corresponding to viscosities ( $\mu_p$ ) of  $1.2$  cP,  $1.4$  cP,  $1.6$  cP, and  $1.8$  cP respectively. Progressing  $0.1$  mm from the stenosis origin, the flow dwindles to  $7.59 \text{ mm}^3/\text{s}$ ,  $6.5 \text{ mm}^3/\text{s}$ ,  $5.69 \text{ mm}^3/\text{s}$ , and  $5.06 \text{ mm}^3/\text{s}$ . Entering the mesa area, spanning from  $0.25$  mm to  $0.75$  mm from the stenosis origin, the flow rate cascades to its nadir at  $1.41 \text{ mm}^3/\text{s}$ ,  $1.21 \text{ mm}^3/\text{s}$ ,  $1.06 \text{ mm}^3/\text{s}$ ,  $0.94 \text{ mm}^3/\text{s}$ . Subsequently, beyond the mesa's edge, the flow revives gradually, echoing the earlier ascent leading to the mesa section. Comparing the mesa segment to a regular artery, there is a about  $90\%$  decrease in volumetric flow rate.

### 5.2.2 Analysis of the core layer volume flow rate

The relationship between volumetric flow rate in the core layer and viscosity is illustrated in Fig. 5a. The maximum volumetric flow rate is recorded at  $48.91 \text{ mm}^3/\text{s}$  for lower viscosity values ( $\mu_p = 1.2$  cP and  $\mu_c = 3.5$  cP), whereas the minimum volumetric flow rate is observed at  $32.90 \text{ mm}^3/\text{s}$  for higher viscosities ( $\mu_p = 1.8$  cP and  $\mu_c = 5$  cP). An augmentation of  $0.6$  cP in peripheral viscosity results in a decline of  $13.36 \text{ mm}^3/\text{s}$  in volumetric flow rate throughout all core layer viscosity. Likewise, a rise of  $1.5$  cP in peripheral viscosity causes a decrease of  $2.65 \text{ mm}^3/\text{s}$  in the volumetric flow rate across all peripheral viscosities.

Let's take a different approach to this, that is, let's look at the volumetric flow in the core layer along the axial length of the stenosis as shown in Fig. 6b. When absence of narrowing occurs, the flow volume within the core showcases a sequence of  $47.8 \text{ mm}^3/\text{s}$ ,  $42.08 \text{ mm}^3/\text{s}$ ,  $37.79 \text{ mm}^3/\text{s}$ ,  $34.45 \text{ mm}^3/\text{s}$ , corresponding to viscosities ( $\mu_p$ ) of  $1.2$  cP,  $1.4$  cP,  $1.6$  cP, and  $1.8$  cP respectively while maintaining the core viscosity at  $\mu_c = 4$ . Progressing  $0.1$  mm from the stenosis origin, the flow volume measures  $33.59 \text{ mm}^3/\text{s}$ ,  $29.79 \text{ mm}^3/\text{s}$ ,  $26.94 \text{ mm}^3/\text{s}$ ,  $24.72 \text{ mm}^3/\text{s}$ , and within the area of the mesa section, located between  $0.25$  mm to  $0.75$  mm from the stenosis origin, the flow volume hits its nadir at  $16.6 \text{ mm}^3/\text{s}$ ,  $15.08 \text{ mm}^3/\text{s}$ ,  $13.94 \text{ mm}^3/\text{s}$ ,  $13.06 \text{ mm}^3/\text{s}$  while maintaining a constant pressure of  $120$  mmHg throughout the stenosis. Subsequently, beyond the mesa section, the flow rate gradually ascends once more, following the same pattern observed up to the mesa segment. The reduction in the rate of flow volume is approximately about  $65\%$ ,  $64\%$ ,  $63\%$ , and  $62\%$ , in the mesa segment when contrasted with the typical artery for viscosity ( $\mu_p$ )  $1.2$  cP,  $1.4$  cP,  $1.6$  cP, and  $1.8$  cP respectively.

### 5.2.3 Analysis of the total volume flow rate

The total volumetric flow rate is the combination of the peripheral and core volumetric flow rates. Fig. 5 b and Fig. 6 c, show the relationship between total volumetric flow rate and viscosity, as well as axial distance, respectively. In Fig. 5 b, the highest volumetric flow rate is registered at  $64.50 \text{ mm}^3/\text{s}$  for lower viscosity values ( $\mu_p = 1.2$  cP and  $\mu_c = 3.5$  cP), while the lowest volumetric flow rate is noted at  $43.29 \text{ mm}^3/\text{s}$  for higher viscosities ( $\mu_p = 1.8$  cP and  $\mu_c = 5$  cP). A boost of  $0.6$  cP in periphery viscosity leads to a reduction of  $18.56 \text{ mm}^3/\text{s}$  in volumetric flow rate across all central layer viscosities. Similarly, an increase of  $1.5$  cP in core viscosity results in a drop of  $2.65 \text{ mm}^3/\text{s}$  in the volumetric flow rate among all periphery viscosities. This leads us to infer that viscosity and volumetric flow rate have an inverse

relationship, with one increasing and the other decreasing. The volumetric flow rate drops due to decreased velocity caused by an increase in viscosity.

Fig. 6 c, depicts the overall volumetric flow rate along the axial direction of the stone's length. If there is no narrowing, the flow volume inside the core displays the following order:  $63.39 \text{ mm}^3/\text{s}$ ,  $55.44 \text{ mm}^3/\text{s}$ ,  $49.48 \text{ mm}^3/\text{s}$ ,  $44.84 \text{ mm}^3/\text{s}$ . These values correspond to viscosities ( $\mu_p$ ) of 1.2 cP, 1.4 cP, 1.6 cP, and 1.8 cP, respectively, with the core viscosity remaining at  $\mu_c = 4$ . As the flow volume advances 0.1 mm from the stenosis origin, it measures  $41.18 \text{ mm}^3/\text{s}$ ,  $36.29 \text{ mm}^3/\text{s}$ ,  $32.63 \text{ mm}^3/\text{s}$ ,  $29.78 \text{ mm}^3/\text{s}$ . In the mesa section, which is situated between 0.25 and 0.75 mm from the stenosis origin, the flow volume reaches its minimum at  $18.01 \text{ mm}^3/\text{s}$ ,  $16.29 \text{ mm}^3/\text{s}$ ,  $15 \text{ mm}^3/\text{s}$ , and  $14 \text{ mm}^3/\text{s}$  while keeping the pressure constant at 120 mmHg throughout the stenosis. Then, past the mesa portion, the flow rate progressively rises again in the same manner observed up to the mesa segment. The total flow volume rate decreases by approximately 71.59%, 70.62%, 69.68%, and 68% in the mesa segment when compared to the standard artery for peripheral viscosity values of 1.2 cP, 1.4 cP, 1.6 cP, and 1.8 cP respectively, with a core viscosity of 4 cP.

#### 5.2.4 Visualization of 3-D figure for volumetric flow rate

In Fig. 7, the richer red tone signifies a greater amount of volumetric flow, while the bluish shade indicates a decrease in volumetric flow intensity. Fig. 7b and Fig. 7c, illustrate the volumetric flow rates of the core layer and the total volumetric flow rates, respectively, with variations in the periphery and core viscosity. Fig. 7a, describes about periphery volumetric flow rate with varying pressure and peripheral viscosity. Comparing the three figures, we can conclude that the volumetric flow rate is larger in the core layer than in the peripheral layer, that viscosity and flow rate are inversely related, and that increasing pressure produces a higher flow rate due to increased velocity.

### 5.3 Shear stress

#### 5.3.1 Peripheral shear stress ratio

Figure 8a, illustrates the correlation between peripheral stress ratios in the presence and absence of stenosis, with varying stenosis heights ranging from 0 to 0.3mm for different peripheral radii. Initially, the ratio remained unity across all radii. Upon reaching a stenosis height of 0.15 mm, the stress ratio escalated to 1.490, 1.437, 1.393, and 1.355 for peripheral radii of 1.1 mm, 1.15 mm, 1.2 mm, and 1.23 mm, respectively. Similarly, at a stenosis height of 0.25 mm, the shear stress ratios were recorded as 2.009, 1.880, 1.776, and 1.691 for the aforementioned radii. As the stenosis height peaked at 0.3 mm, the stress ratio followed suit, reaching values of 2.36, 2.171, 2.022, and 1.901 for radii of 1.1 mm, 1.15 mm, 1.2 mm, and 1.25 mm, respectively. Analysis of the data led to the conclusion that an increase in stenosis height directly correlates with heightened shear stress due to blockage. Conversely, an increase in radius facilitates enhanced blood flow, thereby reducing stress levels. For peripheral radii less than or equal to 1.2 mm, shear stress in the peripheral region doubles compared to the initial stress in the periphery when there is no stenosis for maximum height, potentially leading to arterial wall rupture.

In Fig. 8 b, let's explore the periphery stress ratio variations in the presence and absence of stenosis plotted along the stenosis length for different stenosis heights. In the beginning, in the absence of stenosis, the ratio stood at one. As we move 0.15 mm away from the stenosis origin towards the flow direction, the ratio gradually peaks to 1.298, 1.391, 1.493, and 1.605 considering maximum stenosis heights of 0.2mm, 0.25 mm, 0.3 mm, and 0.35 mm respectively. Within the flat region of trapezoidal stenosis or at the maximum stenotic height, the ratio

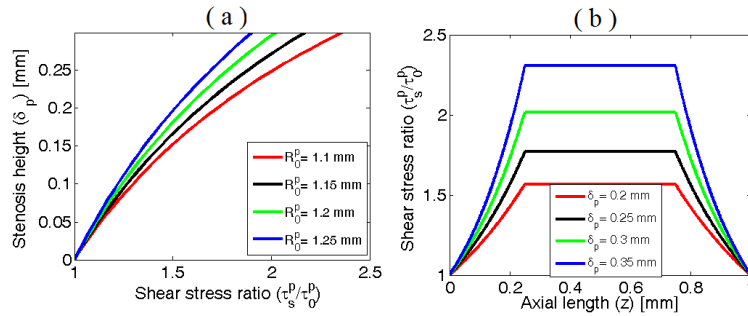


Figure 8: a: Peripheral shear stress ratio for different periphery radii, b: Peripheral shear stress ratio along the axial length for different periphery stenotic height.

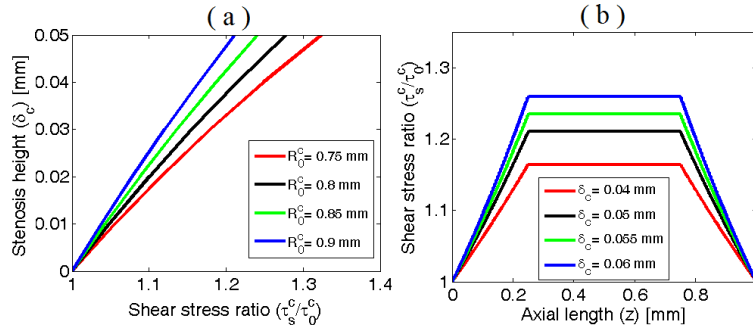


Figure 9: a: Core shear stress ratio for different core radii, b: Core shear stress ratio along axial length for different core stenotic height.

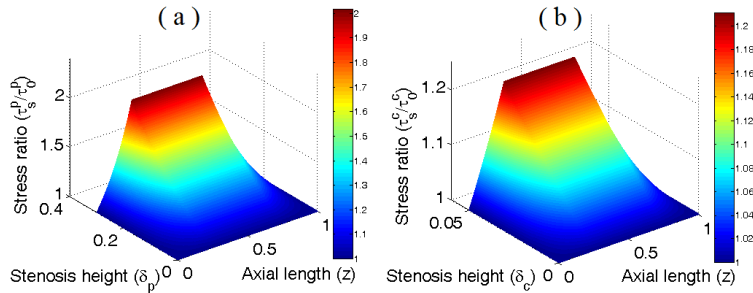


Figure 10: 3-D visualization a: Peripheral shear stress ratio, b: Core shear stress ratio.

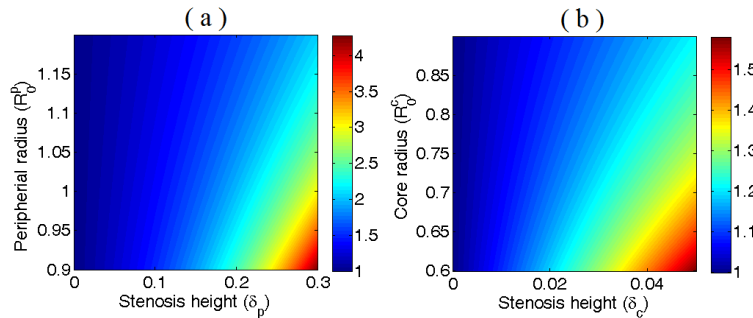


Figure 11: Pressure ratio a: Peripheral pressure ratio, b: Core pressure ratio.

elevates to 1.566, 1.772, 2.022, and 2.306 for the mentioned heights. Subsequently, as we reach the end of the mesa section, the ratio begins to decrease similarly to its earlier increase. In essence, this indicates that the mesa section of the stenosis experiences higher stress levels in comparison to other sections.

### 5.3.2 Core shear stress ratio

Illustration 9 a depicts the connection between core stress ratios when stenosis is present or absent, with stenosis heights ranging from 0 to 0.05 mm for various core radii. Initially, the ratio remained constant across all radii. Upon reaching a stenosis height of 0.015 mm, the stress ratio increased to 1.085, 1.074, 1.066, and 1.058 for peripheral radii of 0.75 mm, 0.8 mm, 0.85 mm, and 0.9 mm, respectively. Similarly, at a stenosis height of 0.035 mm, the shear stress ratios were documented as 1.214, 1.185, 1.162, and 1.143 for the mentioned radii. When the stenosis height peaked at 0.05 mm, the stress ratio also peaked, reaching values of 1.324, 1.278, 1.241, and 1.212 for radii of 0.75 mm, 0.8 mm, 0.85 mm, and 0.9 mm, respectively. Examination of the data concluded that an increase in stenosis height directly corresponds to higher shear stress due to the obstruction. Conversely, an increase in radius enables improved blood circulation, consequently reducing stress levels.

In Fig. 9 b, let's delve into the variations of core stress ratio in the presence and absence of stenosis as plotted along the stenosis length for different stenosis heights. Initially, when there is no stenosis, the ratio remains at one. Moving 0.15 mm away from the stenosis origin towards the flow direction, the ratio gradually increases to 1.094, 1.12, 1.133, and 1.146 with maximum stenosis heights of 0.04 mm, 0.05 mm, 0.055 mm, and 0.06 mm respectively. In the flat region of trapezoidal stenosis or at the maximum stenotic height, the ratio rises to 1.164, 1.212, 1.235, and 1.260 for the mentioned heights. Upon reaching the end of the mesa section, the ratio starts to decrease similarly to its initial rise. Essentially, this suggests that the mesa section of the stenosis encounters higher stress levels compared to other sections.

Fig. 10a and Fig. 10b illustrate a three-dimensional representation showcasing the peripheral stress ratio and core stress ratio as they vary with different periphery and core stenotic heights along the axial length of stenosis respectively. In the peripheral layer, the stenosis height fluctuates between 0 and 0.3 mm, whereas in the core layer, it varies from 0 to 0.05 mm. Here the length of stenosis is 1 mm. The visualization portrays a gradient where the increasing intensity of red hues indicates a higher stress ratio, while the deepening of blue hues signifies a decrease in the shear stress ratio. It is evident from the figures that stress levels peak at the plateau section of the stenosis, and a rise in stenosis height corresponds to an escalation in shear stress experienced at the artery wall.

## 5.4 Pressure drop and its ratio across stenotic artery

The pressure ratios in the peripheral and core layers are shown in Fig. 10a and Fig. 10b, together with the corresponding variations in stenosis height. The rising red hue indicates an increasing pressure ratio, whereas the rising blue hue indicates a decreasing pressure ratio. The peripheral radius ( $R_0^p$ ) moves from 0.9 mm to 1.2 mm in Fig. 10a. When there is no stenosis, the pressure ratio is initially one. The ratio of peripheral pressure with and without stenosis increases gradually as stenosis height increases, implying that when stenosis height increases, pressure would also rise. On the other hand, as the peripheral radius increases, the bluish hue increases as well, indicating a drop in the periphery pressure ratio and possibly a decrease in the pressure within the larger radius arteries. When compared to the corresponding radii for other heights, the maximal stenotic height of 0.3 mm that we measured also has the highest peripheral pressure ratio, which is concerning because pressure increases by nearly 3.5 times greater than it did when there was no stenosis.

Similarly, Fig. 10a, shows the pressure ratio of the core layer with and without stenosis. Here, the radius ( $R_0^c$ ) changes from 0.6 mm to 0.9 mm, while the stenotic height ( $\delta_c$ ) varies from 0 mm to 0.05 mm. The ratio is one at first when there is no stenosis. When compared to an artery without stenosis, the pressure ratio reaches its maximum at a height of 0.05 mm roughly 1.55 times. Based on Fig. 10b, we can conclude that the case will be venerable if the stenotic height is more than 0.04 mm and the core radius is smaller than 0.65 mm. This is because the pressure ratio increases to 1.5 and beyond its original value, forming the senior of rupture in the blood vessel. Comparing both the periphery and core layer pressure ratio simultaneously, we can see that the increase in pressure in the peripheral layer is more rapid than in the core layer in comparison with their respective pressure when there is no stenosis.

## 6 Conclusions

This paper dips into a novel model that illustrates the dynamics of blood flow within a two-layered structure of a narrowed artery. The model hypothesizes that within a cylindrical tube, two layers can be identified: a central core layer containing erythrocytes, and a peripheral plasma layer. To tackle this intricate issue, we expand upon the two-tier blood circulation concept to include trapezoidal-shaped stenosis. This enhanced model allows for the precise calculation of speed patterns, volume flow quantities, pressures, pressure declines, and shear tensions, which are subsequently examined through differing in flow variables. It has been found that viscosity and velocity share an inverse relationship. Additionally, core layer velocity is higher than peripheral layer velocity and changes in peripheral viscosity have a greater effect on core velocity than that of changes in core viscosity. For all viscosities, a 15 mmHg increase in pressure causes the peripheral flow rate to rise by around 13.6%, and the peripheral volumetric flow rate is reduced by approximately 90% when comparing the mesa section to a typical artery as well as core volumetric flow rate also becomes minimum in the top most region of trapezoidal stenosis resulting the total flow rate to become minimum. Moreover, increased stenosis height causes higher shear stress thereby the shear stress is maximum in the plateau part of stenosis but artery size and shear stress have an inverse relationship. The peripheral region experiences a greater rate of stress escalation than the core region. Furthermore, the core pressure ratio increases by more than 1.5 times, while the peripheral pressure ratio rises by 4 times compared to the absence of stenosis. When we compare the pressure ratios of the periphery and core layers concurrently, we may observe that the pressure in the peripheral layer increases more quickly than in the core layer.

## References

- [1] Shipley R.E., Gregg D.E., *The Effect of External Constriction on a Blood Vessel on Blood Flow*, American Journal of Physiology, 141 (1944), 289-296.
- [2] World Health Organisation, *The Atlas of Heart Disease and Stroke*, 2019.
- [3] Crawford K., Jakub K., Lockhart J.S., Wold J.L., *Knowledge, Attitudes, and Beliefs of Cardiovascular Disease Prevention in Young Adults in the Country of Georgia*, Journal of Nursing Scholarship, 5 (2023), 903-913. 10.1111/jnu.12875. Epub 2023 Jan 20. PMID: 36660906.
- [4] Young D.F., *Fluid Mechanics of Arterial Stenosis*, Journal of Biomechanical Engineering, 101 (1979), 157-175. <http://dx.doi.org/10.1115/1.342624>
- [5] Gautam P.N., Pokharel C., Phaijoo G.R., Kattel P., Kafle J., *Effect of Increasing Stenosis Over Time on Hemodynamics*, Biomath, 12.2 (2023), 2310067.
- [6] Merrill E.W., Benis A.M., Gilliland E.R., Sherwood T.K., Salzman E.W., *Pressure-flow relations of human blood in hollow fibers at low flow rates*, Journal of applied physiology, 20.5 (1965), 954-967. <https://doi.org/10.1152/jappl.1965.20.5.954>

- [7] Mann F.C., Herrick J.F., Essex H.E., Blades E.J., *Effects on Blood Flow of Decreasing the Lumen of Blood Vessels*, Surgery, 4 (1938), 249-252.
- [8] Haldar K., *Effects of the Shape of Stenosis on the Resistance to Blood Flow Through an Artery*, Bulletin of Mathematical Biology, 47 (1985), 545-550.
- [9] MacDonald D.A., *On Steady Flow Through Modelled Vascular Stenoses*, Journal of biomechanics, 12.1 (1997), 13-20.
- [10] Chakravarty S., *Effects of Stenosis on the Flow-Behaviour of Blood in an Artery*, International Journal of Engineering Science, 16.4 (1982), 175-180.
- [11] Bitoun J.P., Bellet D., *Blood Flow Through a Stenosis in Micro circulation*, Biorheology, 23.1 (1986), 51-61. <https://doi.org/10.3233/bir-1986-23104>
- [12] Jabbar U.I.A., Ali R.U., Khalid P., Niazi U.H.K., *Three-Dimensional Numerical Analysis of Pulsatile Blood Flow Around Different Plaque Shapes in Human Carotid Artery*, International Journal of Bio-science, Biochemistry and Bioinformatics, 2.5 (2012), 305.
- [13] Liu B., *The Influences of Stenosis on the Downstream Flow Pattern in Curved Arteries*, Medical & engineering physics, 29.8 (2007), 868-876.
- [14] Keshavarz-Motamed Z., Kadem L., *3D Pulsatile Flow in a Curved Tube With Coexisting Model of Aortic Stenosis and Coarctation of the Aorta*, Medical engineering & physics, 33.3 (2011), 315-324.
- [15] Kafle J., Panta K., Gautam P.N., Pokharel C., *Mathematical Analysis of Hemodynamic Parameters of Blood Flow in an Artery*, Mathematics Education Forum Chitwan, 7.7 (2022), 82-91. <https://doi.org/10.3126/mefc.v7i7.54788>
- [16] Bugliarello G., Sevilla J., *Velocity Distribution and Other Characteristics of Steady and Pulsatile Blood Flow in Fine Glass Tubes*, Biorheology, 7.2 (1970), 85-107. <https://doi.org/10.3233/bir-1970-7202>
- [17] Cokelet G.R., *The Rheology of Human Blood*, In *Biomechanics*, Y.C. Fung (Eds.), Prentice-Hall, New Jersey: Englewood Cliffs, 1972.
- [18] Thurston G.B., *Plasma release cell-layering theory for blood flow*, Biorheology, 26 (1972), 199-214.
- [19] Shukla J.B., Parihar, R.S., Gupta S.P., *Effects of Peripheral Layer Viscosity on Blood Flow Through the Artery with Mild Stenosis*, Bulletin of mathematical biology, 42.6 (1980), 797-805. <https://doi.org/10.1007/BF02461059>
- [20] Ponalagusamy R., Manchi R., *A Study on Two-Layered (KL-Newtonian) Model of Blood Flow in an Artery With Six Types of Mild Stenoses*, Applied Mathematics and computation, 367(2020), 124767.
- [21] Chaturani P., Kaloni P.N., *Two-layered poiseuille flow model for blood flow through arteries of small diameter and arterioles*, Biorheology, 13 (1975), 243-250.
- [22] Sing B., Joshi P., Joshi B.K., *Analysis of blood flow through an artery with mild stenosis: a two-layered model*, Italian Journal of Pure and Applied Mathematics, 33 (2014), 35-44.
- [23] Biswas D., Chakraborty U.S., *Two-layered Pulsatile Blood Flow in a Stenosed Artery with Body Acceleration and Slip at Wall*, Applications and Applied Mathematics, 5.2 (2010), 303-320.
- [24] Kapur J.N., *Mathematical Models in Biology and Medicine*, A liated East-West Press Pvt. Ltd., New Delhi, India, 1985.
- [25] Beavers G.S., Joseph D.D., *Boundary Conditions at a Naturally Permeable Wall*, Journal of Fluid Mechanics, 30.1 (1967), 197-207. <http://dx.doi.org/10.1017/S0022112067001375>

Surya Sharma Subedi,  
Institute of Science and Technology,  
Tribhuvan University, Nepal,  
Email: [surya.775509@cdmath.tu.edu.np](mailto:surya.775509@cdmath.tu.edu.np),

Pushpa Nidhi Gautam,  
Patan Multiple Campus,  
Tribhuvan University, Nepal,  
Email: [pushpa.gautam@pmc.tu.edu.np](mailto:pushpa.gautam@pmc.tu.edu.np),

Jeevan Kafle,  
Institute of Science and Technology,  
Tribhuvan University, Nepal,  
Email: [jeevan.kafle@cdmath.tu.edu.np](mailto:jeevan.kafle@cdmath.tu.edu.np)